(12) INTERNATIONAL APPLICATION PUBLISHED UNDER THE PATENT COOPERATION TREATY (PCT)

(19) World Intellectual Property Organization
International Bureau

(43) International Publication Date
01 December 2022 (01.12.2022)

WIPO | PCT

(10) International Publication Number
WO 2022/247672 A1

(51) International Patent Classification:
*C09D 133/08* (2006.01) *C08K 3/015* (2018.01)
*C09D 163/00* (2006.01) *C08K 3/08* (2006.01)
*C09D 175/04* (2006.01) *C08K 3/20* (2006.01)
*C09D 4/04* (2006.01) *C08K 3/36* (2006.01)

(21) International Application Number:
PCT/CN2022/093013

(22) International Filing Date:
16 May 2022 (16.05.2022)

(25) Filing Language: English

(26) Publication Language: English

(30) Priority Data:
63/194,248 28 May 2021 (28.05.2021) US

(71) Applicant: **THE UNIVERSITY OF HONG KONG** [CN/CN]; Pokfulam Road, Hong Kong Special Administrative Region (CN).

(72) Inventors: **WANG, Liqiu**; The University Of Hong Kong, Pokfulam Road, Hong Kong (CN). **LI, Wei**; The University Of Hong Kong, Pokfulam Road, Hong Kong (CN).

(74) Agent: **LIU, SHEN & ASSOCIATES**; 10th Floor, Building 1, 10 Caihefang Road, Haidian District, Beijing 100080 (CN).

(81) Designated States *(unless otherwise indicated, for every kind of national protection available)*: AE, AG, AL, AM, AO, AT, AU, AZ, BA, BB, BG, BH, BN, BR, BW, BY, BZ, CA, CH, CL, CN, CO, CR, CU, CZ, DE, DJ, DK, DM, DO, DZ, EC, EE, EG, ES, FI, GB, GD, GE, GH, GM, GT, HN, HR, HU, ID, IL, IN, IQ, IR, IS, IT, JM, JO, JP, KE, KG, KH, KN, KP, KR, KW, KZ, LA, LC, LK, LR, LS, LU, LY, MA, MD, ME, MG, MK, MN, MW, MX, MY, MZ, NA, NG, NI, NO, NZ, OM, PA, PE, PG, PH, PL, PT, QA, RO, RS, RU, RW, SA, SC, SD, SE, SG, SK, SL, ST, SV, SY, TH, TJ, TM, TN, TR, TT, TZ, UA, UG, US, UZ, VC, VN, WS, ZA, ZM, ZW.

(84) Designated States *(unless otherwise indicated, for every kind of regional protection available)*: ARIPO (BW, GH, GM, KE, LR, LS, MW, MZ, NA, RW, SD, SL, ST, SZ, TZ, UG, ZM, ZW), Eurasian (AM, AZ, BY, KG, KZ, RU, TJ, TM), European (AL, AT, BE, BG, CH, CY, CZ, DE, DK, EE, ES, FI, FR, GB, GR, HR, HU, IE, IS, IT, LT, LU, LV, MC, MK, MT, NL, NO, PL, PT, RO, RS, SE, SI, SK, SM, TR), OAPI (BF, BJ, CF, CG, CI, CM, GA, GN, GQ, GW, KM, ML, MR, NE, SN, TD, TG).

**Published:**
— *with international search report (Art. 21(3))*

(54) Title: SELF-CLEANING PATHOGEN-REPELLENT COATINGS

(57) Abstract: Disclosed is a substrate comprising a pathogen-repellant coating, the pathogen-repellant coating comprising: a haloalkylsilane coated metal and/or metal oxide nanoparticle. Also, disclosed is a method of reducing a spread of a virus, comprising: applying to a surface of a substrate likely to come into contact with virus-bearing droplets a pathogen-repellant coating comprising an adhesive, a haloalkylsilane coated metal and/or metal oxide nanoparticle, and an anti-pathogens additive. Further, disclosed is a pathogen-repellant coating composition, comprising a cyanoacrylate, a perfluorooctyltriethoxysilane and silver nanoparticles.

WO 2022/247672 A1

# SELF-CLEANING PATHOGEN-REPELLENT COATINGS

## TECHNICAL FIELD

Disclosed are virus shielding techniques through liquid repellency and other prevention strategies against, for example, COVID-19.

## BACKGROUND

Since its first report in December 2019, the extremely contagious coronavirus disease 2019 (COVID-19) – caused by the severe acute respiratory syndrome coronavirus 2 (SARS-CoV-2) – has already inflicted over 43 million infections and more than 1 million deaths worldwide by October 2020. Its most common transmission route is direct exposure to virus-laden droplets exhaled during talking, coughing, or sneezing. Another main route is the contact with fomite, infectious source generated after the landing expiratory droplets evaporate on surfaces such as that of doorknob, lift button, and handrail. As viruses in dry nuclei can remain infectious for days on smooth surfaces and even for months at low temperatures, it is critical to minimize the attachment/deposition of virus-laden droplets on the surface.

Personal protective equipment such as surgical mask block the first route through filtration wherein micro-/nano-fiber matrix traps pathogens using inertial and electrostatic forces. However, the filtering efficacy may be offset by the high-momentum cloud flow, a multi-phase flow for 7-8 meters with a velocity peaking at 10-30 m/s produced by sneezes and coughs which carries virus-laden droplets (~1 to 2000 μm in diameter). The insufficiency of current protective techniques is evidenced by a fact that ~6% of the infection cases are front-line medical workers. Additional strategy to reinforce the masking and prohibit droplets retention on frequently touched surfaces, merits untold technological and health care potential, yet remains absent from current anti-viral toolbox. Moreover, substantial

disposable plastics are consumed in biomedical/chemical industries for pathogen testing due to the pathogen residue, especially during pandemics like the COVID-19 pandemic, contributing to worldwide plastic pollution and increasing the risk of pathogen spread.

Prior art like antiviral coating in the market is made of disinfectants with poor hydrophobicity (virus-droplet cannot roll off), which leaves substantial pathogen residue and thus needs longer time for the anti-microbial ingredients to completely inactivate the pathogens (inactivate efficiency only 99% in 1 hour). On the other hand, prior art such as superhydrophobic coatings have potential to repel the bulk of pathogen-laden droplets (virus-droplet quickly rolls off), but trace amount of pathogen residue will inevitably be left on the nanostructures of the coating and such pathogen residue cannot be inactivated because of the lack of anti-microbial additives in the coating. The technologies reported in prior art documents only focus on the superhydrophobic feature of low-surface-energy materials or the inactivation feature of metal/metal dioxides, but the combination of both features remains unexplored. As the metal/metal dioxides are intrinsically hydrophilic, how to coordinate the metal/metal dioxide particles with superhydrophobic materials in order to obtain both repellency and inactivation simultaneously remains challenge to scientists and industry, which is urgently needed to be solved.

## SUMMARY

The following presents a simplified summary of the invention in order to provide a basic understanding of some aspects of the invention. This summary is not an extensive overview of the invention. It is intended to neither identify key or critical elements of the invention nor delineate the scope of the invention. Rather, the sole purpose of this summary is to present some concepts of the invention in a simplified form as a prelude to the more detailed description that is presented hereinafter.

Currently, coronavirus disease 2019 (COVID-19) – a respiratory contagion spreading through expiratory droplets – has evolved into a global pandemic, severely impacting public health and the economy. Herein, personal protection using liquid repellent coatings are described wherein the deposition and penetration of SARS-CoV-2 droplets are prohibited/inhibited. On coated surfaces, SARS-CoV-2 remnants are reduced by seven orders of magnitude, and thus yielding an anti-viral efficacy far outperforming the inactivation rate of disinfectants. The SARS-CoV-2 remnant is found to scale exponentially with the liquid/solid adhesion, uncovering the mechanism and effective means for minimizing SARS-CoV-2 attachment. The novel virus repellent strategy and insight into SARS-CoV-2-surface interaction are of considerable value in fighting the current COVID-19 pandemic and preventing future outbreaks.

Disclosed herein are substrates comprising a pathogen-repellant coating, the pathogen-repellant coating containing an adhesive, a haloalkylsilane coated metal and/or metal oxide nanoparticle, and an anti-pathogens additive.

Also disclosed are methods of reducing a spread of a virus involving applying to a surface of a substrate likely to come into contact with virus-bearing droplets a pathogen-repellant coating comprising an adhesive, a haloalkylsilane coated metal and/or metal oxide nanoparticle, and an anti-pathogens additive.

Further disclosed are pathogen-repellant coating compositions, comprising a cyanoacrylate, a perfluorooctyltriethoxysilane and silver nanoparticles.

To the accomplishment of the foregoing and related ends, the invention comprises the features hereinafter fully described and particularly pointed out in the claims. The following description and the annexed drawings set forth in detail certain illustrative aspects and implementations of the invention. These are indicative, however, of but a few of the various ways in which the principles of the invention may be employed. Other objects, advantages and novel features of the invention will become apparent from the following detailed description of the

invention when considered in conjunction with the drawings.

BRIEF SUMMARY OF THE DRAWINGS

Fig. 1 depicts SARS-CoV-2 repellency. Schematics and chronophotographs of SARS-CoV-2-laden droplets slide/roll on (Fig. 1a) bare glass and (Fig. 1b) surface with a self-cleaning pathogen-repellent coating which combines the repelling effect of a superhydrophobic coating and the inactivation effects brought by anti-microbial additives. Fig. 1c, SARS-CoV-2 gene copy *N* determined through quantitative real-time polymerase chain reaction shows seven orders of magnitude reduction in SARS-CoV-2 retention using the liquid repellent coating. ND represents “not detected” and is denoted by the dashed line. Error bar denotes standard deviation of three independent experiments. Fig. 1d, SARS-CoV-2 retention rate $N_i/N_0$ (denoted by columns) and SARS-CoV-2 repelling rate $(N_0-N_i)/N_0$ (denoted by dots) calculated from (Fig. 1c).

Fig. 2 depicts interfacial virus retention. Fig. 2a, SEM images showing the coatings consisting of $SiO_2$ nanoparticles (SHP and SAP $SiO_2$), soot-templated fractal $SiO_2$ network (SOP $SiO_2$), $TiO_2$ nanoparticles (SHP $TiO_2$), CuO nanoflakes (SHP CuO), and Ag nanocrystals (SHP Ag). Fig. 2b, Chronophotographs showing six rebounds of a 5 μl SARS-CoV-2-laden droplet liberating from a height of ~9 mm on the underlying SOP $SiO_2$ surface. Fig. 2c, SARS-CoV-2-laden droplets have a large contact angle $\theta_{app}$ (> 150˚) and a low roll-off angle $\theta_{roll\text{-}off}$ (< 5˚) for different coating-substrate pairs, but the adhesions $F_{\perp}$ scatters much. Solid and open circles, respectively, denote $\theta_{app}$ and $\theta_{roll\text{-}off}$. Columns denote the vertical liquid/solid adhesion $F_{\perp}$. Error bar denotes standard deviation of three independent experiments. Fig. 2d, The SARS-CoV-2 remnant *N* grows exponentially as the $F_{\perp}$ increases.

Fig. 3 depicts microscale liquid retention. Fig. 3a, Collective pinning of the peripheral local capillary bridges. Red dashed line and purple circles denote

apparent and actual contact lines, respectively. Fig. 3b, Local capillary bridges on microstructured surfaces. Red and purple dashed lines denote the macroscopic and microscopic contact angles, respectively. Fig. 3c, Atop micropost, the capillary bridge recedes as the receding contact angle $\theta_{rec}$ is reached, otherwise, the capillary bridge is pinned and further stretching pinches the bridge, leaving tiny amount of liquid residue. Fig. 3d, Force-displacement curves contrast the maximum $F_{\perp}$ on surfaces capped with pristine and nanotextured microposts. SEM images showing textures of (Fig. 3e) pristine and (Fig. 3f) nanotextured micropost array. Sequential images showing the micro-capillary bridges' receding behaviors on the (Fig. 3g) pristine and (Fig. 3h) nanotextured micropost. Fig. 3i, Fluorescence signals SARS-CoV-2 liquid retention atop pristine microposts. Fig. 3j, No SARS-CoV-2 liquid residues can be detected on the nanotextured microposts.

Fig. 4 depicts sneeze repellency and durability. Fig. 4a, Sequential images showing high-momentum SARS-CoV-2 droplets of simulated sneeze rebound off the SHP $TiO_2$ coated glass. Fig. 4b, Chronophotographs showing the shedding of a ~18 μm SARS-CoV-2 droplet off the surface. Fig. 4c, Abrasion test of the super-repellent coatings on glass, fabric and mask. Error bar denotes standard deviation of three independent experiments. Fig. 4d, Photos contrasting the retention of SARS-CoV-2-loaded droplets on various substrates: glove and mask coated with the SAP $SiO_2$; button, doorknob, and clothing coated with the SHP $SiO_2$.

Fig. 5. depicts the composite anti-viral coating. Fig. 5a, Anti-viral effects of silver nanoparticles (nano Ag) and copper nanoparticles (nano Cu) towards SARS-CoV-2. Fig. 5b, Transmission electron microscope (TEM) image showing the nano Ag with diameter of ~3 nm to ~42 nm. Fig. 5c, SEM images showing the nanostructures of nano Ag-doped SAP $SiO_2$ coating. Fig. 5d, Energy dispersive X-ray spectroscopy (EDX) mapping showing the silver nanoparticles are evenly

distributed in the SAP $SiO_2$ coating. Fig. 5e, The adhesive force $F_{\perp}$, static contact angle $\theta_{app}$ and roll-off angle $\theta_{roll\text{-}off}$ of virus-laden droplet on the SAP $SiO_2$ coating doped with 1%wt nano Ag. Columns denote the vertical liquid/solid adhesion $F_{\perp}$. Solid and open circles, respectively, denote $\theta_{app}$ and $\theta_{roll\text{-}off}$. Error bar denotes standard deviation of three independent experiments. Fig. 5f, The super-repellency of the coating to SARS-CoV-2 is largely maintained regardless of the participation of nano Ag. Columns denote the SARS-CoV-2 gene copy $N$ and open circles denote the SARS-CoV-2 repelling rate $(N_0\text{-}N_i)/N_0$. Error bar denotes standard deviation of three independent experiments.

Fig. 6 depicts the characterization of the self-cleaning pathogen-repellent coating readily applied on diverse substrates. Fig. 6a, SEM image showing the morphology of the coating. Fig. 6b, EDX mapping showing the silver nanoparticles are evenly distributed in the coating. Fig. 6c, TEM image showing the nanostructures of the coating. Fig. 6d, Contact angles of inactivated SAR-CoV-2 droplet on the coating and SEM images of the coating on diverse substrates. Fig. 6e, The effect of silver nanoparticle concentration on contact angle, repelling rate and inactivation rate. Fig. 6f, The durability of the coating is verified by sandpaper abrasion.

## DETAILED DESCRIPTION

Infectious diseases such as coronavirus disease 2019 (COVID-19) are highly efficient in person-to-person transmission. To prevent their spread, we use self-cleaning pathogens-repellent coatings both to block direct exposition to the pathogen-laden fluid droplets (droplets containing viruses, bacteria, fungi, protozoa, or worms) and to minimize their attachment to the surfaces of e.g., the personal protection equipment (PPE) and frequently touched objects such as doorknobs. Unlike masks which protect people from infection by filtration during

respiration, or disinfectants which inactivate the pathogens after pathogens deposition, the pathogen-repellent coating minimizes virus attachment/deposition via directly repelling pathogens-containing droplets in the first place. By incorporating anti-pathogens additives such as silver nanoparticles into the coating, the trace amount of residual pathogens is further inactivated.

The most common transmission route of infectious disease like COVID-19 is direct exposure to pathogens-laden droplets exhaled during talking, coughing, or sneezing. Another important route is the contact with "fomite", infectious source generated after the pathogen-laden droplets evaporate on surfaces such as that of doorknob, lift button, and handrail. As pathogens such as severe acute respiratory syndrome coronavirus 2 (SARS-CoV-2) on metal, glass, wood, fabric, and plastic surfaces can remain infectious for several hours to days, preventing their spread is extremely challenging. To reduce the risk of infection, it is critical to eliminate the deposit of pathogen-laden droplets. Moreover, it is estimated that disposable plastics worth US$20 billion are consumed annually in biomedical/chemical testing. The used plastics are left with potentially infectious pathogens residues and hazardous wastes that cost another US$10 billion to handle. We use self-cleaning pathogen-repellent coatings both to block direct exposition to the pathogens-laden fluid droplets and to minimize their attachment to the surfaces of e.g. the personal protection equipment (PPE) and frequently touched objects such as doorknobs, thus reducing the risk of infection and reducing the usage of disposable plastics.

Described herein is the new use for reducing the risk of infection and reducing the usage of disposable plastics by minimizing pathogens attachment to diverse surfaces.

As indicated, the present invention refers to substrates comprising a pathogen-repellant coating, the pathogen-repellant coating containing an adhesive, a haloalkylsilane coated metal and/or metal oxide nanoparticle, and an anti-pathogens additive.

As used herein, the term “pathogen-repellant coating” or “self-cleaning pathogen-repellent coating” refers to a coating which demonstrates both repelling and inactivation effects against pathogen.

The self-cleaning pathogen-repellent coatings include superhydrophobic (SHP), superamphiphobic (SAP), and superomniphobic (SOP) types, fabricate by functionalizing diverse nanostructures, including $SiO_2$ nanoparticles (SHP and SAP $SiO_2$), soot-templated fractal $SiO_2$ network (SOP $SiO_2$), $TiO_2$ nanoparticles (SHP $TiO_2$), CuO nanoflakes (SHP CuO), and Ag nanocrystals (SHP Ag).

For simplicity, nanostructures, nanoparticles, nanoflakes, and nanocrystals can be referred to as nanoparticles. The nanoparticles have a size suitable to minimizing pathogens attachment to diverse surfaces so treated. In one embodiment, the nanoparticles have a size where at least about 95% by weight have a size from about 1 nm to about 100 nm. In this connection, size refers to average cross-section of a particle, such as diameter. In another embodiment, the nanoparticles have a size where at least about 95% by weight have a size from about 1 nm to about 70 nm. In yet embodiment, the nanoparticles have a size where at least about 95% by weight have a size from about 1.5 nm to about 50 nm. In still yet embodiment, the nanoparticles have a size where at least about 95% by weight have a size from about 2 nm to about 25 nm.

The adhesive ensures the bonding of the coating to diverse substrates. Suitably, the adhesive is selected from one or more of an acrylic resin, an epoxy resin, a polyurethane, and a cyanoacrylate. The adhesive can be bound to diverse substrate at ambient condition, under drying and/or curing condition. As used herein, curing condition can refer to heating and/or radiation, suitably heating at no more than 100℃.

The haloalkylsilane coated metal and/or metal oxide nanoparticle contributes to the formation of hydrophobic structures/surfaces. As used herein, the term “haloalkylsilane coated” means that at least partial of the nanoparticle

surface is coated with haloalkylsilane compound.

Suitably, the haloalkylsilane is selected from one or more of a perfluorodecyltriethoxysilane, a perfluorodecyltrichlorosilane, a perfluorooctyltriethoxysilane, an octadecyltrichlorosilane, a perfluorohexyltrichlorosilane, a perfluorooctyltrichlorosilane, and a perfluorodecanethiol.

The nanoparticles contain one or more metal and/or metal oxide of silicon oxide, copper, copper oxide, zinc, zinc oxide, silver, silver oxide, titanium, and titanium oxide.

The anti-pathogens additive imparts the coating with inactivation effect against pathogen. Suitably, the anti-pathogens additive comprises at least one of silver nanoparticles, copper nanoparticles, zinc nanoparticles, zinc oxide nanoparticles and titanium dioxide nanoparticles. Suitably, the anti-pathogens additive comprises at least silver nanoparticles.

The anti-pathogens additive can be present of about 0.1% to about 0.7% by weight, preferably 0.2-0.6% by weight based on the solid/dry weight of the coating.

When the silver nanoparticle content is less than 0.1% by weight, the coating is in superhydrophobic sate, which exhibits high repelling rate but lacks inactivation ability. When content of silver nanoparticles is higher than 0.7% by weight, the coating turns into hydrophilic state, which exhibits high inactivation rate but lacks repelling ability.

The haloalkylsilane coated metal and/or metal oxide nanoparticle and the anti-pathogens additive can comprise about 55-80% by weight based on the solid/dry weight of the coating.

The haloalkylsilane coated metal and/or metal oxide nanoparticle and the anti-pathogens additive can have the size ratio of about 0.3-1.5.

The self-cleaning pathogen-repellent coating shows super repellency to fluids loaded with diverse pathogens (contact angle >150°, roll-off angle <5°),

including viruses, bacteria, fungi, protozoa, and worms. The pathogen-laden fluid on the coating beads up like a marble and readily rolls without residue.

The self-cleaning pathogen-repellent coating not only repels pathogen-laden droplets (repelling efficiency of as high as 99.99999%) due to its super repellency but also inactivates the trace amount of residual pathogens (inactivation efficacy of about 90%, even as high as 99.99%) because it contains anti-pathogens additives like silver/copper nanoparticles.

The self-cleaning pathogen-repellent coating can adapt to various substrates with contrasting composition, texture, and geometry. The substrate can be one or more selected from glass, polyester fabric, steel, copper, mask, nitrile glove, and paper.

The pathogen-repellent coating is self-cleaning as it can remove any dirt or pathogens on it.

The following one or more problems are at least partially solved by the disclosure herein.

As pathogens such as severe acute respiratory syndrome coronavirus 2 (SARS-Co V-2) on metal, glass, wood, fabric, and plastic surfaces can remain infectious for several hours to days, preventing their spread is extremely challenging. Tough disinfectants could inactivate the pathogens on surface, they often require relatively longer time to reach an effective inactivation rate (e.g. 99.9% in 1 hour) because of the substantial pathogen residues caused by poor hydrophobicity, and lose efficacy quicky due to evaporation or contamination.

The filtering efficacy of personal protective equipment such as surgical mask may be offset by the high-momentum cloud flow, a multi-phase flow for 7-8 meters with a velocity peaking at 10-30 m/s produced by sneezes and coughs which carries pathogen-laden droplets. Additional strategy to reinforce the masking is required.

Huge amount of disposable plastics are consumed in biomedical/chemical industries for pathogen testing, estimated to be US$20 billion annually. The used

plastics are left with potentially infectious pathogens residues, increasing the risk of pathogens spread and producing a lot of hazardous waste, which costs another US$10 billion to handle.

The problems are at least partially solved by one or more of the following.

The use of a self-cleaning pathogen-repellent coating to prohibit the deposition of pathogens on diverse surfaces by directly repelling the potential pathogens-containing droplets in the first place without any residue, yielding an anti-pathogens efficacy as high as 99.99999%, a value far outperforms the inactivation rate of disinfectants. In other embodiments, the anti-pathogens efficacy is at least 99.99%, at least 99.999%, or at least 99.9999%.

The use of a self-cleaning pathogen-repellent coating to reinforce the mask as it prohibits liquid delivery and resists high-momentum droplet impact.

The use of a self-cleaning pathogen-repellent coating to eliminate the pathogens residues on the surface of diverse equipment used for pathogen testing, such as pipet, test tube, and dropper, thus reducing the usage of disposable plastics and increasing environmental safety.

The fabrication of the self-cleaning pathogen-repellent coating in some embodiments is a multi-step process and time-consuming.

Pinpointing the fluidic transmission nature, the techniques described herein exploit liquid repellency for the upgrade of anti-viral protection as it prohibits liquid delivery and resists high-momentum droplet impact. For superhydrophobic (SHP) surface, aqueous droplet preferentially resides atop micro-/nano-textures wherein the sparse liquid/solid contacts promote interfacial detachments. By introducing re-entrant micro-/nano-structures and special low-surface-energy polymers, the surface can be made repellent to both water and oil, termed superamphiphobicity (SAP), or even nearly all types of liquids, termed superomniphobicity (SOP). Upon impact, liquid penetration attempt is thwarted by the nanoscopic porosity, building a shield towards the pathogen-bearing droplets. However, to date, the exact repelling efficacy of liquid-repellent surfaces

against SARS-CoV-2 remains unexamined and the interaction between the two has not yet been explored.

Six types of non-wetting surfaces are fabricated on a large materials gamut, including glass, fabric, steel, copper, mask, nitrile glove, and paper. It is found that they have the super repellency to droplets loaded with SARS-CoV-2. We traced viral residue along droplets' rolling trails and find that SARS-CoV-2 remnants are reduced by seven orders of magnitude, a value outperforms the inactivation rate of disinfection procedure and the filtration efficiency of mask. More importantly, we uncover a fact that the amount of SARS-CoV-2 remnant grows exponentially with the increasing of liquid/solid adhesion, capillary force parameterized by pinned fractions $\phi$ (depending on physical textures) and receding contact angles $\theta_{rec}$ (depending on surface chemistry). Such virus repelling strategy and the understanding of interaction between virus solution and solid will be valuable for our combat against the current COVID-19 pandemic as well as future epidemics.

For example, a 50 μl virus-laden droplet, containing $1\times10^7$ PFU $ml^{-1}$ viable SARS-CoV-2 on bare and coated substrates. After five minutes, the substrates are tilted for 90° to remove any unattached solution and the SARS-CoV-2 remnants on contact regions are probed using quantitative real-time polymerase chain reaction (qRT-PCR). Daily encountered materials, including glass, fabric (polyester), steel, copper, mask, nitrile glove, and paper, are chosen as substrates. Six types of repellent coatings, including superhydrophobic (SHP), superamphiphobic (SAP), and superomniphobic (SOP) types, are fabricated by functionalizing diverse nanostructures, including $SiO_2$ nanoparticles (SHP and SAP $SiO_2$), soot-templated fractal $SiO_2$ network (SOP $SiO_2$), $TiO_2$ nanoparticles (SHP $TiO_2$), CuO nanoflakes (SHP CuO), and Ag nanocrystals (SHP Ag). The substrate and coating are paired on the basis of their compatibility.

Unlike the firmly pinned droplets on pristine glass (Fig. 1a), on coated surface, the virus solution minimizes the contact by forming a spherical droplet

and rolls off the repellent slope in a frictionless manner, meanwhile the pathogen being contact with silver nanoparticles is inactivated (Fig. 1b). As such, the self-cleaning pathogen-repellent coating of the invention by adding trace amounts of disinfectants (less than 1 wt%) like silver nanoparticles into specific superhydrophobic coating materials, not only repels nearly all incoming pathogen-laden droplets with a repelling rate as high as 99.99999% but also inactivates the residue pathogens with an inactivation rate as high as 99.99%, which is unprecedently achieved by either conventional superhydrophobic coatings or disinfectants.

As shown in Fig. 1c,d, we quantify the retention of SARS-CoV-2 $N_i$ (virus gene copy) on different coating-substrate pair and detect a substantial reduction as high as seven orders of magnitude compared with that of the bare substrate $N_0$, generating a repelling rate $(N_0-N_i)/N_0$ as high as 99.99999%, a value surpassing the filtration rate of the N95 mask (e.g. 95%) and inactivation rate of the chemical disinfectant (e.g. 99.9% in 1 hour). For the evaluated materials, superior repelling performance generally conserves except for nitrile glove overlaid with SHP $SiO_2$ and SHP $TiO_2$. Such failure is potentially caused by the coating exfoliation, a consequence of the poor interfacial bonding between the rigid coating and elastic plastic sheet. The SARS-CoV-2 repellency has some levels of variation across different substrates, as observed that the performance of the SHP $SiO_2$ coating peaks for paper but degrades on other substrates, signaling a pairwise optimization between the coating and substrates properties such as the textures and flexibility.

As shown in Fig. 2a, the scanning electron microscopy (SEM) image delineates the nanoscale topography whose geometry and interfacial chemistry work in concert to reduce the liquid/solid adhesion and consequently the liquid retention. As shown in Fig. 2b, the nano-textures effectively withstand the impact of a SARS-CoV-2 droplet (Weber number = 5.5), as observed that the droplet rebounds for more than six times before its final rest, acting as a soft elastic

object. For different coating-substrate pairs, the virus-bearing droplets all exhibit a large contact angle (> 150°) and a low roll-off angle (< 5°), minimizing the liquid/solid contact and maximizing the in-plane liquid mobility (Fig. 2c). The similar contact angles for different coating-substrate pairs indicate that the virus remnant is relatively independent of the substrate static wettability. Using a microforce sensing probe, we measure the vertical liquid adhesive force $F_{\perp}$ between the SARS-CoV-2 solution and coating. Unlike the wettability, the $F_{\perp}$ scatters for different pairs (Fig. 2c). On glasses coated with SAP $SiO_2$, $F_{\perp}$ is only 0.29 μN. However, the force peaks at 59.37 μN on nitrile glove coated with SHP $SiO_2$, a wide range spanning three orders of magnitude. By plotting data in logarithmic axis (Fig. 2d), the fitting between *N* and $F_{\perp}$ unfolds an interesting exponential relationship as $N \propto 1.26^{F_{\perp}}$, implying a rapid growth rate of *N* as $F_{\perp}$ increases. Given the fact that the transmission of SARS-CoV-2 is highly efficient, it is key to reduce the interfacial adhesion towards SARS-CoV-2-laden droplets to minimize the infection risk.

Such interfacial adhesion originates in the capillary bridges formed atop the nanotextures. To sidestep the structural irregularities, we assume that the coating caps isotropic nanopost array on the substrate. Along the apparent contact line, nano-capillary bridges form (Fig. 3a). Individual peripheral nano-capillary bridge generates a vertical force of $\oint_s \gamma \sin\theta^{n} ds - \Delta P \times (\pi a^2/4)$, where γ is the liquid surface tension, $\theta^{n}$ is the local contact angle along the nanopost perimeter *s*, Δ*P* is the Laplace pressure that relates to droplet radius *R* as 2γ/*R*, and *a* is the diameter of the nanopost (Fig. 3b). The contribution from Laplace pressure is usually an order of magnitude smaller than that from the surface tension, and thus reducing the force into $\oint_s \gamma \sin\theta^{n} ds$. The local contact angle $\theta^{n}$ is smaller along the outer edge of the nanopost than that along the interior edge.

As a SARS-CoV-2 droplet departs the surface, nano-capillary bridges stretch, gradually reducing the outermost $\theta^n$. Once the local $\theta^n$ reaches the intrinsic receding contact angle, the contact line recedes atop the nanopost (Fig. 3c). Depending on the parameters such as droplet's velocity and stretching angles, the capillary bridge eventually detaches the post through absolute receding or partial pinch-off, potentially leaving diminutive residues. Such liquid remnants retain SARS-CoV-2 on the surfaces and are too diminutive to be quantified with available techniques, especially on the irregular nanostructures with super-repellency. A pristine and a nanotextured micropost array is fabricated as modelled surfaces to study the correlation between $F_\perp$ and liquid residues (Fig. 3e,f).

The overall adhesion is collectively contributed by the dynamics of all capillary bridges along the apparent contact line. Paxson *et al.* propose an effective pinned fraction $\phi$, defined as the ratio of the length of actual peripheral contact line to the apparent one as $ns/l_{app}$, where n is the number of peripheral capillary bridges and $l_{app}$ is the apparent contact line length. Such pinning is self-similar at micro- and nano-scale. On isotropic nanopost array, the pinned fraction $\phi$ is determined by the pitch $\tau$ as $s/\tau$. By simply assuming that the localized contact angle atop the nanopost is the intrinsic receding contact angle $\theta_{rec}$, the vertical adhesive force can be simplified as $F_\perp = \phi l_{app} \gamma \sin\theta_{rec}$. For sparsely distributed sharp nanostructures, the pinned fraction $\phi^n$ can be as low as ~0.1. Thus, the pinned fraction $\phi^m$ are much higher on pristine microposts than that of the nanotextured microposts ($\phi^m \phi^n$). As expected and shown in Fig. 3d, the $F_\perp$ of SARS-CoV-2 droplet on pristine microposts surpass the nanotextured microposts by 89.66 μN (Fig. 3e,f). Side view in Fig. 3g shows that the $\theta_{rec}$ on the pristine micropost is so small that the value cannot be obtained by stretching the capillary bridge. As a result, the liquid bridge undergoes pinch-off and leaves substantial SARS-CoV-2 liquid residue atop the pristine micropost. However, the nanoscale

coating significantly increases the microscale $\theta_{rec}$ to be nearly 150°, so that the contact line can readily recede on nanotextured micropost without obvious pinning (Fig. 3h). Further fluorescence imaging in Fig. 3i, j contrasts the expected dyed SARS-CoV-2 solution residues where residue is observed atop the pristine micropost and absent in the nanotextured one. Thus, to prohibit the liquid retention and subsequently the SARS-CoV-2 remnants, we must decrease $\phi$ by designing the hierarchical roughness and increase $\theta_{rec}$ by decreasing the surface energy, two critical parameters depicting the interfacial adhesion.

Testing the utility involves simulating an interaction between a sneeze and the repellent coating. As shown in Fig. 4a, inactivated-SARS-CoV-2-laden droplets of sizes ranging from ~10 to ~1000 μm are sprayed towards a glass slide coated with the SHP $TiO_2$ coating through an airbrush. A large SARS-CoV-2 droplet with a diameter of 1021 μm impinges the surface at 4.8 ms and immediately rebounds at 10.6 ms. At the end of the violent spraying (105.2 ms), a diminutive SARS-CoV-2 droplet with a diameter of ~18 μm can still be effectively shed off, maintaining the hygiene and cleanness of the surface (Fig. 4b). We also test the mechanical durability of different coatings using sandpaper and find that the coatings' performance basically maintains for up to 100 abrasion cycles (Fig. 4c). It becomes counter-intuitive as some coating such as SAP $SiO_2$ on fabric becomes more virally-repellent after abrasion. We hypothesize that such effect is caused by additional micro-scale roughness introduced by the abrasion which further improve the liquid repellency. Then frequently touched objects such as glove, mask, button, doorknob, and clothing are treated with the repellent coating (Fig. 4d). Coated objects exhibit excellent repellency which confirms that the coating can adapt to various substrates with contrasting composition, texture, and geometry, showing its potential for wide applications.

Anti-viral ingredients can be also incorporated into the super-liquid-repellent coatings to form composite anti-viral coatings that both repel and inactivate virus. Silver nanoparticle (nano Ag) and copper nanoparticles (nano Cu)

have been exploited as anti-pathogens agents. However, their effects against SARS-CoV-2 are mostly unknown. We then first examine the anti-viral efficiency of nano Ag (~15 nm) and nano Cu (~60 nm) towards SARS-CoV-2. As shown in Fig. 5a, both nano Ag and nano Cu demonstrate remarkable anti-SARS-CoV-2 effect as evidenced by the significantly reduced infectious SARS-CoV-2 virus particles, which is determined by $TCID_{50}$ assays. Specifically, nano Cu demonstrated a 10-fold decrease in infectious SARS-CoV-2 titer and nano Ag demonstrated a 426-fold decrease in infectious SARS-CoV-2 titer.

Because of the outstanding anti-SARS-CoV-2 property of nano Ag and super-repellency of SAP $SiO_2$ coating, we then evaluate the virus repellent effect of nano Ag doped SAP $SiO_2$ coating (SAP $SiO_2$+1% nano Ag) by performing virus adhesion test. As shown in Fig. 5b, the size of nano Ag ranges from ~3 nm to ~42 nm. Adding 1%wt nano Ag into the SAP $SiO_2$ coating has no effect on the morphology of coating (Fig. 5c) and the nano Ag is homogeneously distributed in the composite coating (Fig. 5d). As shown in Fig. 5e, f, the 1% nano Ag doped $SiO_2$ coating largely retains its SARS-CoV-2 repellent capacity on diverse substrates except for nitrile glove. Such failure may be caused by the coating exfoliation as the hydrophilic nano Ag may weaken the interfacial bonding between SAP $SiO_2$ coating and elastic plastic sheet. The results demonstrate that nano Ag is an effective anti-viral agent against SARS-CoV-2 and the composite anti-viral coating that both repels and inactivates virus can be prepared by introducing anti-viral additives like nano Ag into the super-liquid-repellent coating.

In another embodiment, the self-cleaning pathogen-repellent coating is prepared from a coating composition, comprising a cyanoacrylate, a perfluorooctyltriethoxysilane and silver nanoparticles. This coating can be readily applied to nearly all kinds of surface. Suitably, the silver nanoparticles are in the range of 0.2-0.6% by weight based on the total weight of the coating composition.

This coating readily applied on diverse substrates was tested for characterization. As shown in Fig. 6a-c, numerous nanostructures increase the roughness of the coating and thus provide the coating with superhydrophobicity. The silver nanoparticles are homogenously distributed in the coating and will be effective to inactivate the residual pathogens. As shown in Fig. 6d, the coating can be readily applied to diverse substrates, including glass, fabric, steel, copper, mask, paper and gloves. The superhydrophobicity is further evidenced by the ultra-high contact angles of the inactivated SAR-CoV-2 droplet on the coating. However, the superhydrophobicity of the coating gradually decays with the increase of the silver nanoparticles content because the silver nanoparticles are intrinsically hydrophilic (Fig. 6e). When the silver nanoparticle content is less than 0.1 wt%, the coating is in superhydrophobic sate, which exhibits high repelling rate but lacks inactivation ability. When content of silver nanoparticles is higher than 0.7 wt%, the coating turns into hydrophilic state, which exhibits high inactivation rate but lacks repelling ability. As a result, the content of silver nanoparticles is crucial for the coating to obtain both repelling and inactivation performance simultaneously. Our invention shows that repelling rate as high as 99.99999% and inactivation rate as high as 99.99% can be simultaneously achieved by the coating with the mass fraction of silver nanoparticles ranging from 0.2% to 0.6% by weight. We then test the mechanical durability of the coatings by performing sandpaper abrasion. The result shows that the micro-textures of the coatings are largely retained after the sandpaper abrasion and thus the coatings' virus-repellent functionality can essentially maintain up to 100 abrasion cycles (Fig. 6f).

Infection prevention and control of pandemic are critical to human existence, considering the fact that our society is constantly battered by widespread infectious diseases, for example, the outbreak of severe acute respiratory syndrome (SARS) in 2003, Middle East respiratory syndrome (MERS) in 2012, and now the COVID-19. Here, we demonstrate that using super-liquid-

repellent coating, the SARS-CoV-2-laden droplets can be effectively repelled, an effective and efficient way to block the two aforementioned main routes of SARS-CoV-2 transmission. The SARS-CoV-2 remnants scale exponentially with the liquid/solid adhesion, showing the key role played by the liquid/solid adhesion in reducing the virus remnants. Overall, the innovative SARS-CoV-2 prevention strategy demonstrated in this study can be widely applied, and can thus play an essential role to fight the current COVID-19 pandemic and prevent future outbreaks.

Methods

Materials. 1*H*,1*H*,2*H*,2*H*-perfluorodecyltrichlorosilane (PFDTS) (97%) was purchased from Gelest. 1*H*,1*H*,2*H*,2*H*-perfluorodecyltriethoxysilane (>98.0%) and tris(hydroxymethyl)aminomethane (>99.0%) were purchased from Tokyo Chemical Industry Corporation. 1*H*,1*H*,2*H*,2*H*-perfluorooctyltriethoxysilane (98%), 1*H*,1*H*,2*H*,2*H*-perfluorodecanethiol (97%), silver nitrate (≥99.0%), tetraethyl orthosilicate (TEOS) (≥99%), dichloromethane (≥99.5%), and fluorescein isothiocyanate (FITC)-BSA (FITC-BSA) were purchased from Sigma-Aldrich. Sodium hydroxide (97%) and potassium persulfate (≥99.0%) were purchased from J&K Scientific. Ammonium hydroxide (28 to 30% in water) and hydrochloric acid (37% in water) were purchased from Acros. Silica nanoparticles (15 nm) was purchased from Shanghai Maikun Chemical Co., Ltd., China. Titanium oxide nanoparticles (99.8%, anatase, ~100 nm) was purchased from Macklin. Sylgard 184 silicone elastomer kit was purchased from Dow Corning. Ethanol (absolute) was purchased from VWR International. Deionized water was produced by a deionized water system (DINEC, Hong Kong). Commercial glass slide, polyester fabrics, steel sheet, copper sheet, mask, nitrile gloves and printing paper are cut into ~2cm×2cm.

Virus and biosafety

SARS-CoV-2 HKU-001a was isolated from the nasopharyngeal aspirate specimen of a laboratory-confirmed COVID-19 patient in Hong Kong as we previously described. The virus was titered in VeroE6 cells with plaque assays as we previously described. All experiments involving live SARS-CoV-2 followed the approved standard operating procedures of the Biosafety Level 3 facility at the Department of Microbiology, University of Hong Kong. The inactivated SARS-CoV-2 virus solution was prepared by incubating the virus in 4% paraformaldehyde. The lack of infectious titer was confirmed with median tissue culture infectious dose (TCID50) assays on VeroE6 cells.

Viral adhesion test.

50 µl of droplet with SARS-CoV-2 at a concentration of 1×107 PFU ml-1 was applied to bare or coated surface. After 5 minutes, the surfaces were 90 degree-tilted to allow free falling of the virus droplet. Each surface was then added with 5 ml of phosphate-buffered saline (PBS) and was incubated for 30 minutes before harvesting for viral RNA extraction.

Virus residue detection using fluorescence imaging

The 10-µl probe liquid [fluorescein isothiocyanate (FITC)-BSA (5 mg ml−1) in inactivated SARS-CoV-2 virus solution] was released to allow rolling on the tested surface. The droplets' traces were observed by fluorescence imaging using an inverted fluorescence microscope (Nikon Eclipse, TS100) equipped with a high-speed camera (Phantom, M110). The fluorescence of FITC-BSA was excited by a 490-nm light source.

RNA extraction and quantitative real time reverse transcription polymerase chain reaction (qRT-PCR)

The virus-containing PBS solution was lyzed with equal volume of AVL buffer and was subsequently extracted for total RNA with the QIAamp viral RNA

mini kit (Qiagen, Hilden, Germany). Quantitative real-time one-step qRT-PCR was used for quantitation of residual SARS-CoV-2 using the QuantiNova Probe RT-PCR kit (Qiagen) with a LightCycler 480 Real-Time PCR System (Roche, Basel, Switzerland) as we previously described. The primers and probe sequences were against the RNA-dependent RNA polymerase/Helicase (RdRP/Hel) gene region of SARS-CoV-2: Forward primer: 5'-CGCATACAGTCTTRCAGGCT-3'; Reverse primer: 5'-GTGTGATGTTGAWATGACATGGTC-3'; SARS-CoV-2 specific probe: 5'-FAM-TTAAGATGTGGTGCTTGCATACGTAGAC-IABkFQ-3'.

$TCID_{50}$ assay for anti-viral effects of silver and copper nanoparticles

In order to test the anti-viral effect of copper and silver nanoparticles, 500 µl of SARS-CoV-2 virus stock ($1\times10^7$ PFU $ml^{-1}$) were mixed with 500 µl of 1000 ppm copper nanoparticles, silver nanoparticles, or $H_2O$. The mixtures were incubated for 24 hours at 4 ℃ to allow full contact of viral particle and nanoparticle. At the same time, VeroE6 cells were seeded in 96 well plates at the concentration of $2\times10^4$ per well. After 24 hours of incubation, the infectious titers of the virus-containing mixtures were quantified with $TCID_{50}$ assays. In brief, the virus-containing mixtures were serially-diluted with DMEM only medium. The diluted mixtures were added to VeroE6 cells and infectious titers were quantified at 72 hours post infection.

Fabrication of SHP $SiO_2$ coated surfaces

The substrate was first treated with spray adhesive (3M Super 75) to enhance robustness of the coating. A mixture of 10 g commercial spray, Glaco (Soft99), and 0.01g silver nanoparticles was then used to render substrate to be superhydrophobic by spray coating. Coated surface was then baked at 80 ºC for 30 min to enhance inter-particle binding.

Fabrication of SAP $SiO_2$ coated surfaces

The suspension of polysiloxane/silica was prepared through hydrolytic condensation of 1*H*,1*H*,2*H*,2*H*-perfluorodecyltriethoxysilane and TEOS in the presence of silica nanoparticles. Firstly, silica nanoparticles (0.1 g) were dispersed in a solution containing 44 ml ethanol and 6ml ammonia aqueous solution. The mixture was ultrasonicated for 30 min. Then 1*H*,1*H*,2*H*,2*H*-perfluorodecyltriethoxysilane (150 µl) and TEOS (150 µl) were injected with vigorous stirring at 600 rpm. After reaction at room conditions for 24 hours, the polysiloxane/silica suspension was formed. Copper nanoparticles (0.01g) was added into the suspension to improve the disinfection ability of the coating. The substate was then treated with spray adhesive (3M Super 75) to enhance the robustness of the coating. By spray coating the suspension (10 ml) onto vertically placed substrate using an airbrush (Paasche H-SET) with 0.2 MPa nitrogen, the superamniphobic surface was prepared.

Fabrication of SOP $SiO_2$ coated surfaces

The superomniphobic surface was prepared by modifying the previously reported superamphiphobic surface based on candle soot. The glass slide (Luoyang Tengjing glass Co. Ltd) was first coated with candle soot, and then placed in a desiccator together with 1 ml of tetraethoxysilane and 1 ml of ammonia hydroxide. The desiccator was closed, and the vacuum was maintained for 18 hours. Then, the carbon soot core was removed by annealing at 550 °C for 3 hours in an oven. The annealed sample was treated with air plasma for 5 min using a plasma cleaner (Harrick, PDC-002-HP) at a high power (45W). The sample was deposited with PFDTS (100 µl) in vacuum for 2 hours to decrease its surface energy. The sample was then heated at 130 ºC for 30 min to remove the unreacted PFDTS, followed by heat treatment at 310 ºC for 15 min.

Fabrication of SHP $TiO_2$ coated surfaces

To prepare the superhydrophobic $TiO_2$ solution, 1.0 g of 1*H*,1*H*,2*H*,2*H*-perfluorooctyltriethoxysilane was placed into 99 g of absolute ethanol, and the solution was mechanically stirred for 2 hours. To the resulting solution, 6 g of titanium oxide nanoparticles and 6 g of Degussa P25 titanium oxide and 0.1g silver nanoparticles were added to make a paint-like suspension. The substate was then treated with spray adhesive (3M Super 75) to enhance the robustness of the coating. In the following experiments, a syringe needle is used to paint the substrate, and the paint was then dried in air for 20 min.

Fabrication of SHP CuO coated surfaces

The copper sheet was ultrasonically cleaned in ethanol and deionized water for 10 min, respectively, followed by washing with diluted hydrochloric acid (1 M) for 10 s to remove the native oxide layer. Then the copper sheet was immersed in a freshly mixed aqueous solution of 2.5 mol $l^{-1}$ sodium hydroxide and 0.1 mol $l^{-1}$ potassium persulfate at room temperature for 60 min, followed by thorough rinsing with deionized water and drying in a nitrogen stream. As a result of chemical etching, CuO nanoflakes with an average diameter ~3.0 µm were produced. The sample was deposited with PFDTS (100 µl) in vacuum for 20 min to decrease its surface energy, followed by heat treatment at 150 ºC in air for 2 h to render surface superhydrophobic.

Fabrication of SHP Ag coated surfaces

To fabricate the silver-nanocrystal-based superhydrophobic surface, the polished copper sheet was first cleaned through successive ultrasonic rinses in ethanol, acetone, and isopropanol, and then under nitrogen flow. Silver nanostructures were deposited onto the copper by immersing the copper sheet into aqueous silver nitrate solution (0.01 mol $l^{-1}$) for 45 s. Then, the sheet was washed with deionized water and dried under nitrogen flow. Then, fluorinated self-assembly monolayer was deposited onto the surface by immersing the sheet

into a 1*H*,1*H*,2*H*,2*H*-perfluorodecanethiol in dichloromethane solution (0.001 mol $l^{-1}$) for 15 min. The fabrication was completed by washing the surface with fresh dichloromethane and drying in ambient condition for 5 min.

Fabrication of PDMS micropost surface

The negative mold consisting of the hole array (diameter ~80 μm, depth ~60 μm, pitch ~230 μm) was first fabricated on a silicon wafer (<100> type) with a thickness of 420 ± 5 μm by standard photolithography. PDMS precursor containing 10 weight % (wt %) curing agent (Sylgard 184 silicone elastomer kit) was thoroughly stirred and vacuumed for 1 hour to remove internal gas. The prepared PDMS was then casted on the negative mold and vacuumed for 1 hour, followed by curing at 80 ºC for 1 hour. The PDMS micropost surface was obtained after peeling the PDMS out from the mold. The nano-textured PDMS micropost surface was prepared by spray-coating the SAP $SiO_2$ solution onto the PDMS micropost surface.

Fabrication of the self-cleaning pathogen-repellent coatings readily applied on various substrates

Solutions of methyl-2-cyanoacrylate (1.0g), silver nanoparticles (0.004g) and 1H,1H,2H,2H-perfluorodecyltriethoxysilane (0.02g) was prepared in 100 ml of acetone. The solution was mechanically stirred for 2 hours. By spray coating the suspension (10 ml) onto vertically placed substrate using an airbrush (Paasche H-SET) with 0.2 MPa nitrogen, the self-cleaning pathogen-repellent coatings was prepared. No further treatment is needed.

Characterizations

The physical structures of the coatings were imaged using a Hitachi S4800 scanning electron microscope. Energy-dispersive X-ray scattering was used to obtain the elemental mapping of various elements in super-repellent

coatings. The measurements of contact angles were conducted using a goniometer (DataPhysics, OCA 25). Contact angle measurements were implemented by depositing a small droplet of liquid (~5 μl) onto the surface using a 1-ml syringe (Hamilton) equipped with a dosing needle of 0.23 mm in outer diameter. The roll-off angles were measured by tilting a stage until the droplet (~5 μl) started to roll off the surface. The adhesive forces on diverse surfaces were measured using a tensiometer (DataPhysics, DCAT 25) by compressing and then retracting a 10 μl droplet. For the measurement, the droplet is attached to a metal holder of 2.5 mm in diameter and pressed onto the surface with a compression distance of 0.5 mm. Afterwards the droplet is pulled off until detachments from the surfaces. The force-displacement diagram is being recorded and the adhesive force is then calculated using the maximum force. Averages from at least three independent measurements are used.

Abrasion test

In the abrasion test, the super-repellent surfaces were placed facedown to the sandpaper (Standard glasspaper, 2000 cw). The surfaces were longitudinally abraded for 2 cm by the sandpaper under a pressure of ~0.2 kPa and then abraded backward for another 2 cm. This process is defined as 1 cycle. The virus residue test was conducted after abrasion for 50 cycles and 100 cycles.

Unless otherwise indicated in the examples and elsewhere in the specification and claims, all parts and percentages are by weight, all temperatures are in degrees Centigrade, and pressure is at or near atmospheric pressure.

With respect to any figure or numerical range for a given characteristic, a figure or a parameter from one range may be combined with another figure or a parameter from a different range for the same characteristic to generate a numerical range.

Other than in the operating examples, or where otherwise indicated, all numbers, values and/or expressions referring to quantities of ingredients, reaction conditions, etc., used in the specification and claims are to be understood as modified in all instances by the term "about."

While the invention is explained in relation to certain embodiments, it is to be understood that various modifications thereof will become apparent to those skilled in the art upon reading the specification. Therefore, it is to be understood that the invention disclosed herein is intended to cover such modifications as fall within the scope of the appended claims.

## CLAIMS

1. A substrate comprising a pathogen-repellant coating, the pathogen-repellant coating comprising:

an adhesive, a haloalkylsilane coated metal and/or metal oxide nanoparticle, and an anti-pathogens additive.

2. The substrate comprising a pathogen-repellant coating according to claim 1, wherein the haloalkylsilane is selected from one or more of a perfluorodecyltriethoxysilane, a perfluorodecyltrichlorosilane, a perfluorooctyltriethoxysilane, an octadecyltrichlorosilane, a perfluorohexyltrichlorosilane, a perfluorooctyltrichlorosilane, and a perfluorodecanethiol.

3. The substrate comprising a pathogen-repellant coating according to claim 1 or 2, wherein the adhesive is selected from one or more of an acrylic resin, an epoxy resin, a polyurethane, and a cyanoacrylate.

4. The substrate comprising a pathogen-repellant coating according to any one of claims 1-3, wherein the anti-pathogens additive comprises at least one of silver nanoparticles, copper nanoparticles, zinc nanoparticles, zinc oxide nanoparticles and titanium dioxide nanoparticles, preferably silver nanoparticles.

5. The substrate comprising a pathogen-repellant coating according to any one of claims 1-4, wherein the content of the anti-pathogens additive is from about 0.1% to about 0.7% by weight, preferably 0.2-0.6% by weight based on the solid/dry weight of the coating.

6. The substrate comprising a pathogen-repellant coating according to any

one of claims 1-5, wherein the substrate has at least one of a superhydrophobic surface, a superamphiphobic surface, and a superomniphobic surface.

7. The substrate comprising a pathogen-repellant coating according to any one of claims 1-6, wherein the pathogen-repellant coating comprises at least one of superhydrophobic $SiO_2$ nanoparticles, superamphiphobic $SiO_2$ nanoparticles, a superomniphobic soot-templated fractal $SiO_2$ network, superhydrophobic $TiO_2$ nanoparticles, superhydrophobic CuO nanoflakes, and superhydrophobic Ag nanocrystals.

8. The substrate comprising a pathogen-repellant coating according to any one of claims 1-7, wherein the metal and/or metal oxide nanoparticle comprises at least one of silicon oxide, copper, copper oxide, zinc, zinc oxide, silver, silver oxide, titanium, and titanium oxide.

9. The substrate comprising a pathogen-repellant coating according to any one of claims 1-8, wherein the metal and/or metal oxide nanoparticle comprises at least two of silicon oxide, copper, copper oxide, zinc, zinc oxide, silver, silver oxide, titanium, and titanium oxide.

10. The substrate comprising a pathogen-repellant coating according to any one of claims 1-9, wherein the nanoparticles have a size where at least about 95% by weight have a size from about 1 nm to about 100 nm.

11. The substrate comprising a pathogen-repellant coating according to any one of claims 1-10, wherein the haloalkylsilane coated metal and/or metal oxide nanoparticle and the anti-pathogens additive have the size ratio of 0.3-1.5.

12. The substrate comprising a pathogen-repellant coating according to

any one of claims 1-11, wherein the haloalkylsilane coated metal and/or metal oxide nanoparticle and the anti-pathogens additive comprise 55-80% by weight based on the solid/dry weight of the coating.

13. The substrate comprising a pathogen-repellant coating according to any one of claims 1-12, wherein the substrate is selected from glass, polyester fabric, steel, copper, mask, nitrile glove, and paper.

14. The substrate comprising a pathogen-repellant coating according to any one of claims 1-13, wherein the substrate is selected from a doorknob, a lift button, and a handrail.

15. The substrate comprising a pathogen-repellant coating according to any one of claims 1-14, having an anti-pathogens efficacy of at least 99.999%.

16. The substrate comprising a pathogen-repellant coating according to any one of claims 1-15, having an inactivation rate of at least 90%.

17. The substrate comprising a pathogen-repellant coating according to any one of claims 1-16, wherein an aqueous virus-bearing droplet on a surface of the substrate exhibits a contact angle of at least 150° and a roll-off angle of less than 5°.

18. A method of reducing a spread of a virus, comprising:

applying to a surface of a substrate likely to come into contact with virus-bearing droplets a pathogen-repellant coating comprising an adhesive, a haloalkylsilane coated metal and/or metal oxide nanoparticle, and an anti-pathogens additive.

19. The method according to claim 18, further comprising:

heating the coated substrate at a temperature from 40 ºC to 90 ºC for a sufficient period of time to facilitate binding of the pathogen-repellant coating to the substrate.

20. The method according to claim 18 or 19, wherein the pathogen-repellant coating is applied to the surface of the substrate by spray coating an aqueous solution of metal and/or metal oxide nanoparticles and a haloalkylsilane.

21. The method according to any one of claims 18-20, wherein the pathogen-repellant coating is applied to the surface of the substrate by depositing a paint-like suspension of a haloalkylsilane and metal and/or metal oxide nanoparticles in an alcohol, then drying.

22. The method according to any one of claims 18-21, wherein the pathogen-repellant coating is applied to the surface of the substrate by dipping the substrate into a dichloromethane solution of a haloalkylsilane and metal and/or metal oxide nanoparticles.

23. The method according to any one of claims 18-22, further comprising:

applying an adhesive to the surface of the substrate prior to applying the pathogen-repellant coating.

24. A pathogen-repellant coating composition, comprising a cyanoacrylate, a perfluorooctyltriethoxysilane and silver nanoparticles.

25. The pathogen-repellant coating composition according to claim 24, wherein the silver nanoparticles is in the range of 0.2-0.6% by weight based on the solid/dry weight of the coating.

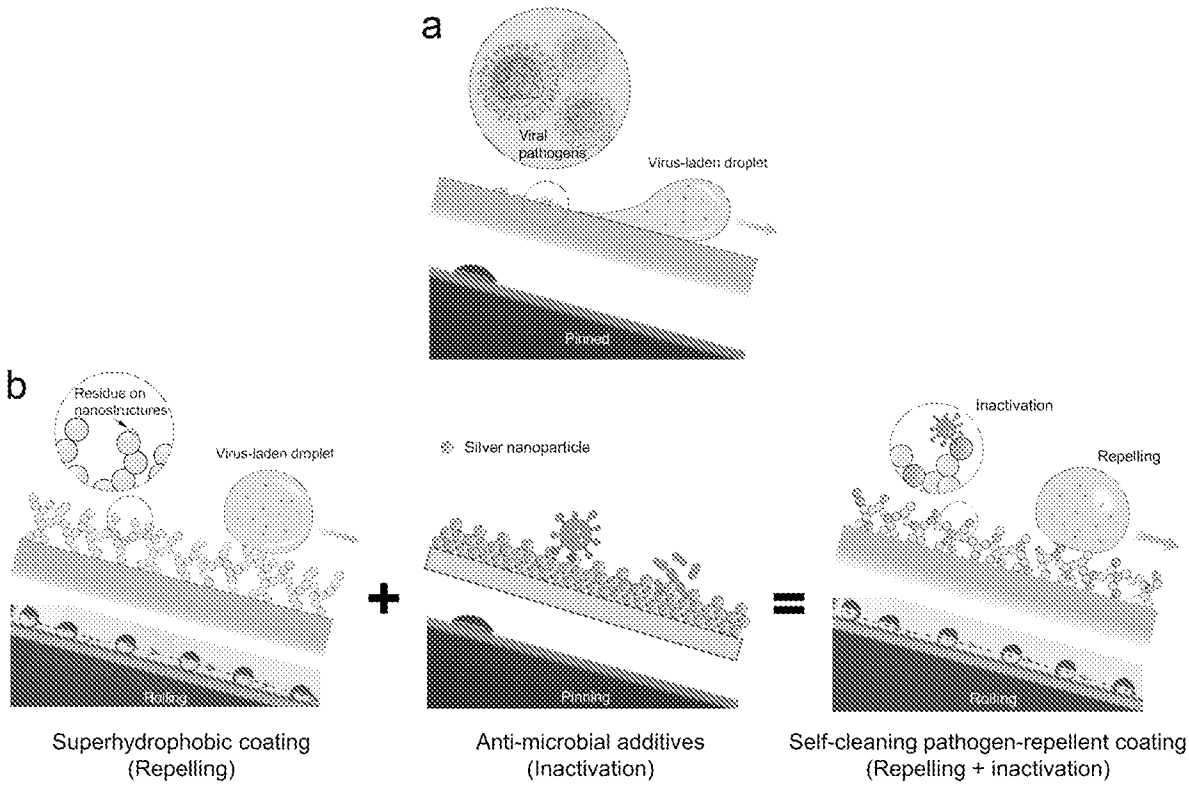
a
Viral pathogens
Virus-laden droplet
Polluted
b
Residue on nanostructures
Virus-laden droplet
Silver nanoparticle
Inactivation
Repelling
Polluted
Polluted
Polluted
Superhydrophobic coating (Repelling)
Anti-microbial additives (Inactivation)
Self-cleaning pathogen-repellent coating (Repelling + inactivation)

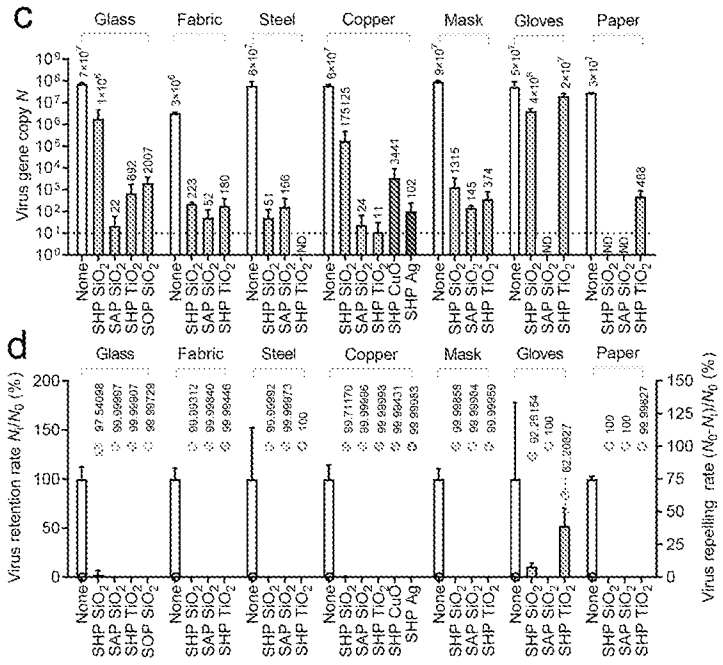
c
Glass
Fabric
Steel
Copper
Mask
Gloves
Paper
Virus gene copy N
None
SHP SiO2
SAP SiO2
SHP TiO2
SOP SiO2
SHP CuO
SHP Ag
ND
d
Virus retention rate Nt/N0 (%)
Virus repelling rate (N0-Nt)/N0 (%)

Fig. 1

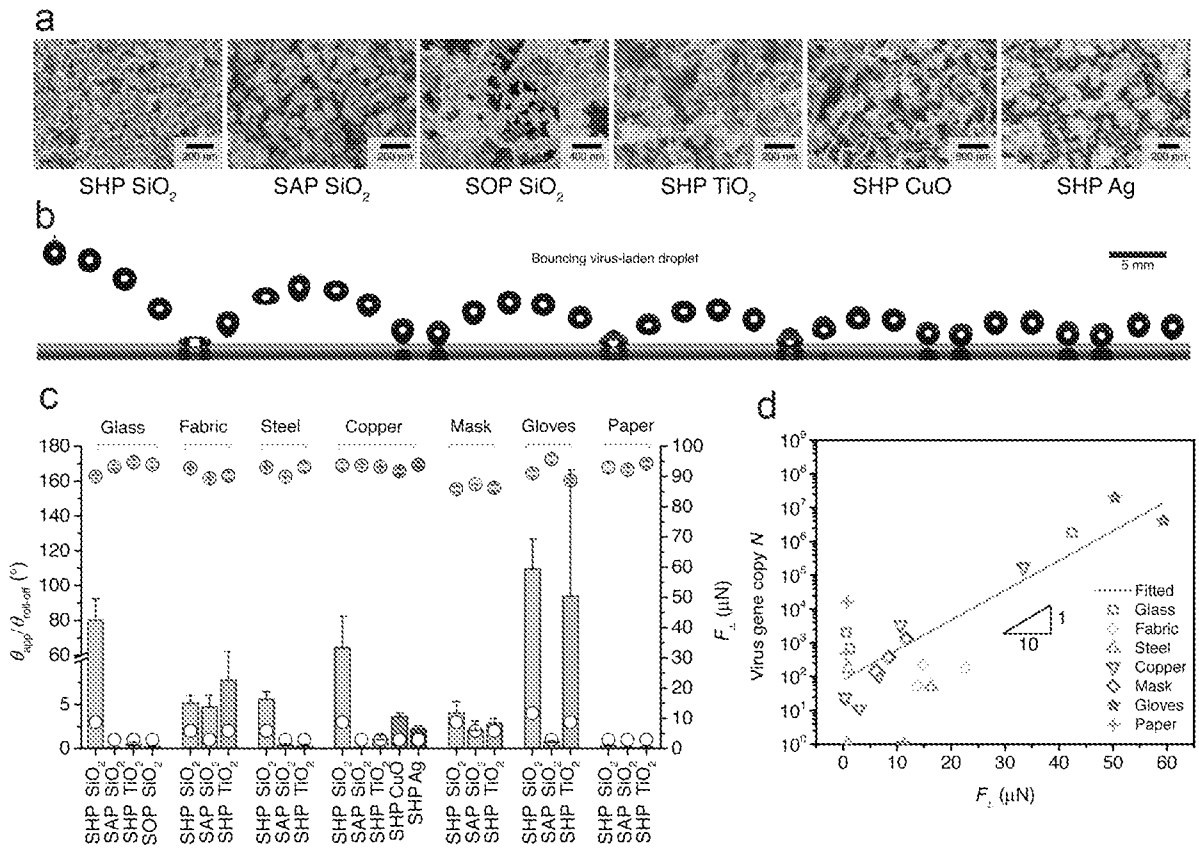
a
SHP SiO2
SAP SiO2
SOP SiO2
SHP TiO2
SHP CuO
SHP Ag
b
Bouncing virus-laden droplet
5 mm
c
Glass
Fabric
Steel
Copper
Mask
Gloves
Paper
θadv/θrol-off (°)
F⊥ (μN)
SHP SiO2
SAP SiO2
SHP TiO2
SOP SiO2
SHP CuO
SHP Ag
d
Virus gene copy N
F⊥ (μN)
Fitted
Glass
Fabric
Steel
Copper
Mask
Gloves
Paper
1
10

Fig. 2

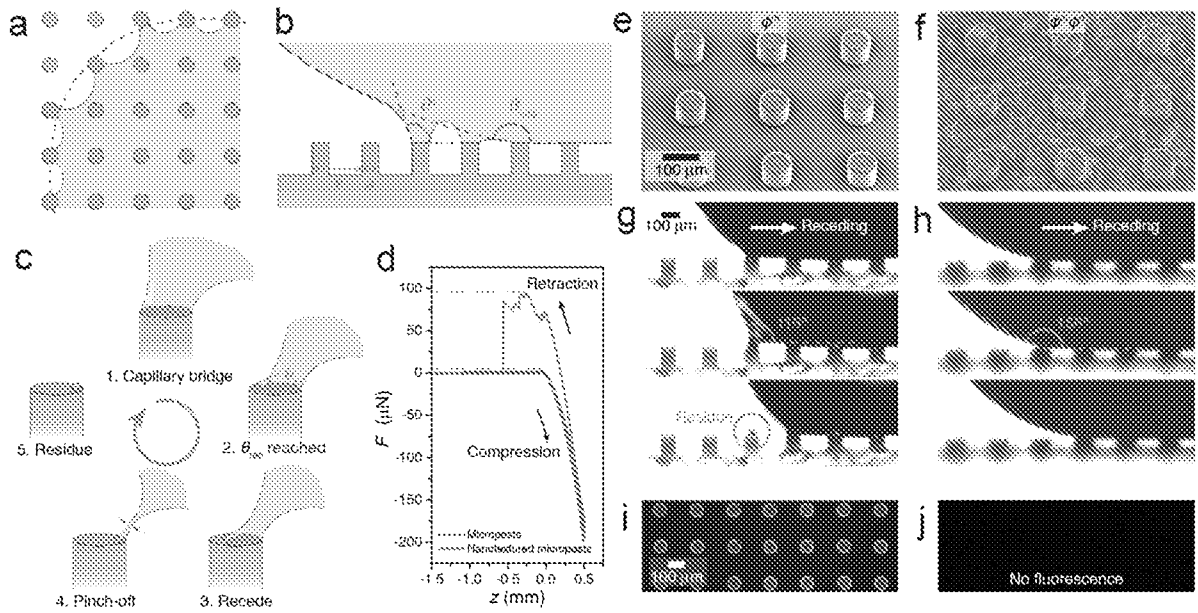
a
b
c
d
e
f
g
h
i
j
1. Capillary bridge
2. $\theta_{ac}$ reached
3. Recede
4. Pinch-off
5. Residue
Retraction
Compression
F (μN)
z (mm)
Micropaste
Nanoreduced micropaste
100 μm
Receding
No fluorescence

Fig. 3

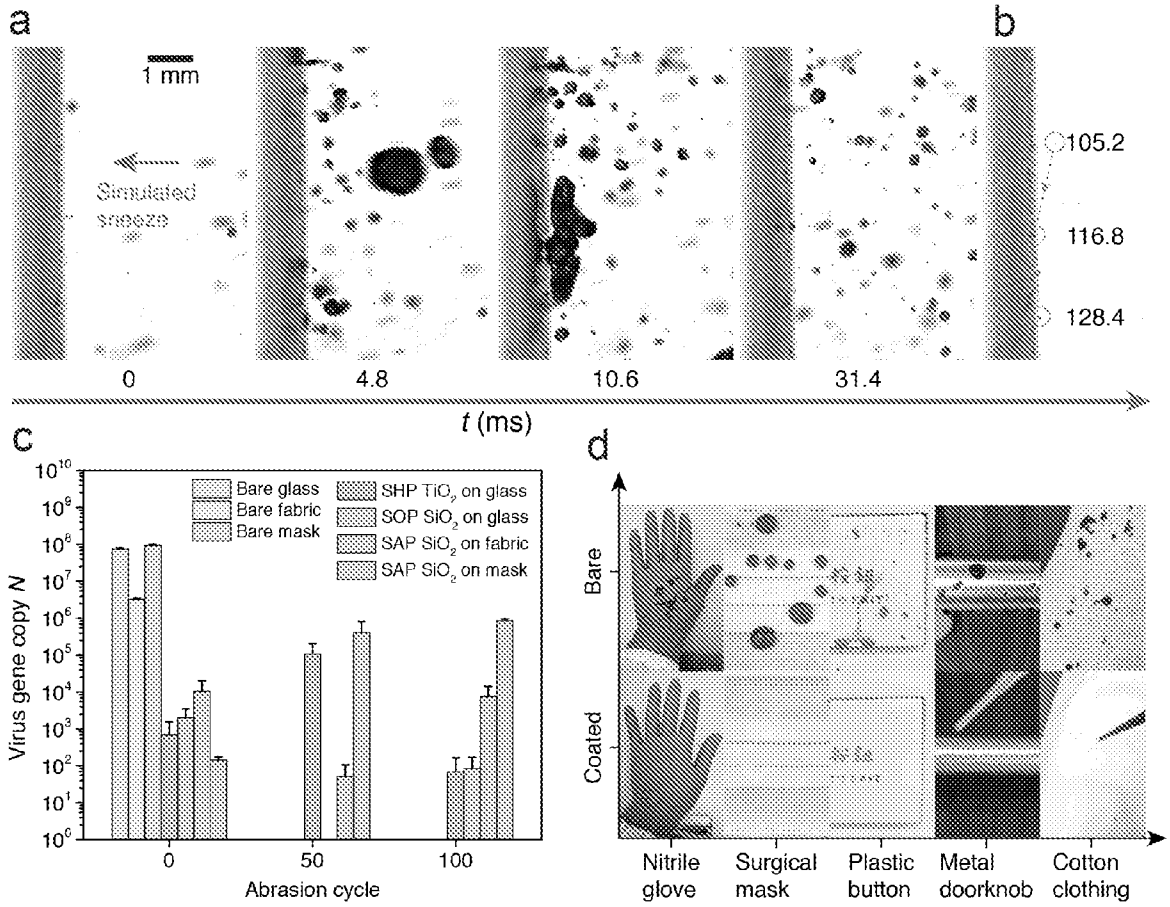
a
1 mm
Simulated sneeze
0
4.8
10.6
31.4
t (ms)
b
105.2
116.8
128.4
c
Virus gene copy N
Bare glass
Bare fabric
Bare mask
SHP TiO2 on glass
SOP SiO2 on glass
SAP SiO2 on fabric
SAP SiO2 on mask
0
50
100
Abrasion cycle
d
Bare
Coated
Nitrile glove
Surgical mask
Plastic button
Metal doorknob
Cotton clothing

Fig. 4

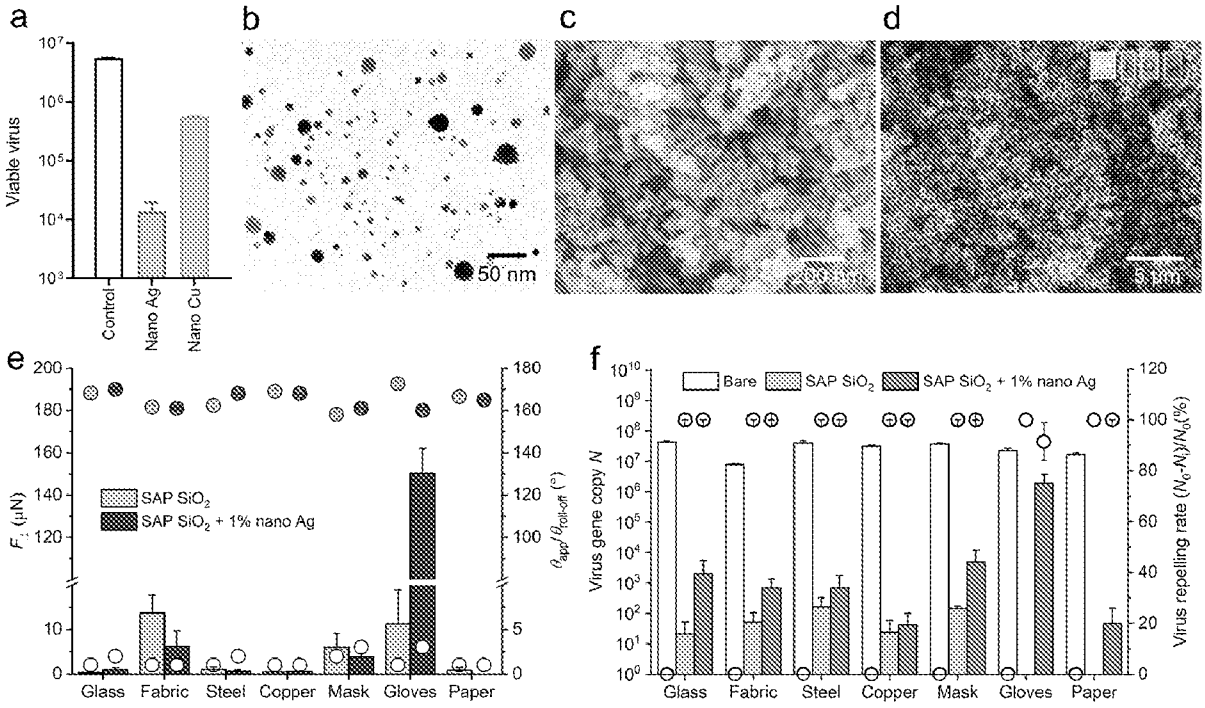
a
b
c
d
Viable virus
Control
Nano Ag
Nano Cu
50 nm
e
f
SAP SiO2
SAP SiO2 + 1% nano Ag
Bare
Glass
Fabric
Steel
Copper
Mask
Gloves
Paper
Virus gene copy N
Virus repelling rate (N0-N)/N0(%)

Fig. 5

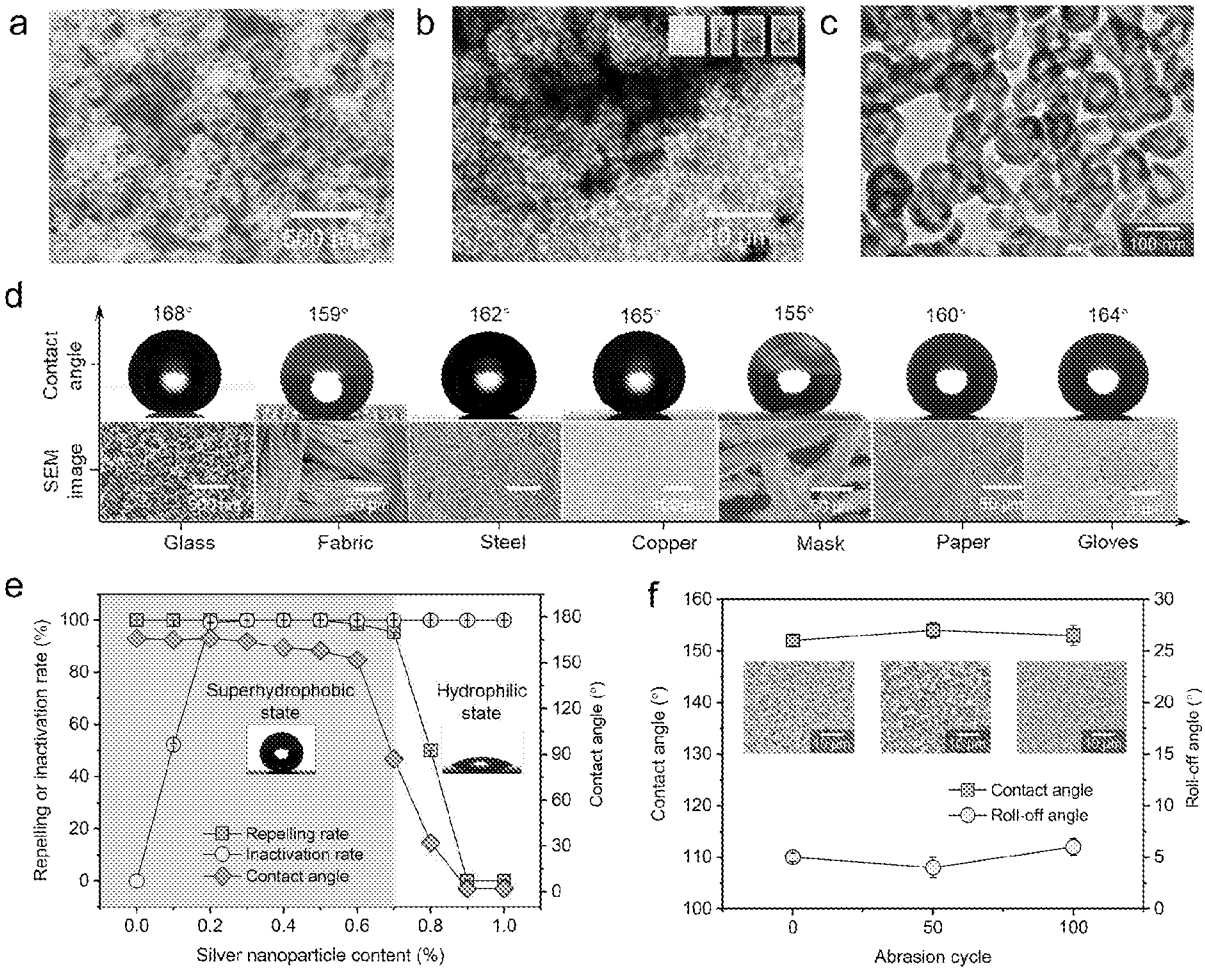
a
b
c
d
168°
159°
162°
165°
155°
160°
164°
Contact angle
SEM image
Glass
Fabric
Steel
Copper
Mask
Paper
Gloves
e
Repelling or inactivation rate (%)
Contact angle (°)
Superhydrophobic state
Hydrophilic state
Repelling rate
Inactivation rate
Contact angle
Silver nanoparticle content (%)
f
Contact angle (°)
Roll-off angle (°)
Contact angle
Roll-off angle
Abrasion cycle

Fig. 6

# INTERNATIONAL SEARCH REPORT

International application No.
**PCT/CN2022/093013**

## A. CLASSIFICATION OF SUBJECT MATTER

C09D 133/08(2006.01)i; C09D 163/00(2006.01)i; C09D 175/04(2006.01)i; C09D 4/04(2006.01)i; C08K 3/015(2018.01)i; C08K 3/08(2006.01)i; C08K 3/20(2006.01)i; C08K 3/36(2006.01)i

According to International Patent Classification (IPC) or to both national classification and IPC

## B. FIELDS SEARCHED

Minimum documentation searched (classification system followed by classification symbols)

C09D133, C09D163, C09D175, C09D4, C08K3

Documentation searched other than minimum documentation to the extent that such documents are included in the fields searched

Electronic data base consulted during the international search (name of data base and, where practicable, search terms used)

DWPI, CNTXT, WPABS, CNKI: coating, coat, paint, adhesive, +pathogen, +bacterial, +microbial, antibiosis, sterilization, sterilisation, silver, Ag, copper, Cu, zinc, Zn, ZnO, titanium, TiO2, silicon dioxide, SiO2, fluoro, fluorine, silane

## C. DOCUMENTS CONSIDERED TO BE RELEVANT

| Category* | Citation of document, with indication, where appropriate, of the relevant passages | Relevant to claim No. |
|---|---|---|
| Y | CN 106467685 A (CHENGDU NASHUO SCI & TECHNOLOGY CO LTD) 01 March 2017 (2017-03-01)<br>paragraphs 0002-0010 in description | 1-25 |
| Y | CN 107033650 A (CHERY AUTOMOBILE CO LTD) 11 August 2017 (2017-08-11)<br>paragraphs 005-0022 in description | 1-25 |
| Y | CN 103443042 A (CORNING INC) 11 December 2013 (2013-12-11)<br>claims 1-32 | 1-25 |
| Y | CN 110283529 A (UNIV SICHUAN) 27 September 2019 (2019-09-27)<br>claims 1-10 | 1-25 |
| Y | CN 111185170 A (GUANGDONG HONGSHULIN NEW MATERIAL TECHNOLOGY CO LTD) 22 May 2020 (2020-05-22)<br>claims 1-10 | 1-25 |
| A | CN 110407482 A (UNIV QINGDAO TECHNOLOGY) 05 November 2019 (2019-11-05)<br>claims 1-10 | 1-25 |

☐ Further documents are listed in the continuation of Box C. ☑ See patent family annex.

* Special categories of cited documents:
"A" document defining the general state of the art which is not considered to be of particular relevance
"E" earlier application or patent but published on or after the international filing date
"L" document which may throw doubts on priority claim(s) or which is cited to establish the publication date of another citation or other special reason (as specified)
"O" document referring to an oral disclosure, use, exhibition or other means
"P" document published prior to the international filing date but later than the priority date claimed
"T" later document published after the international filing date or priority date and not in conflict with the application but cited to understand the principle or theory underlying the invention
"X" document of particular relevance; the claimed invention cannot be considered novel or cannot be considered to involve an inventive step when the document is taken alone
"Y" document of particular relevance; the claimed invention cannot be considered to involve an inventive step when the document is combined with one or more other such documents, such combination being obvious to a person skilled in the art
"&" document member of the same patent family

| Date of the actual completion of the international search | Date of mailing of the international search report |
|---|---|
| **15 August 2022** | **22 August 2022** |
| Name and mailing address of the ISA/CN<br>**National Intellectual Property Administration, PRC**<br>**6, Xitucheng Rd., Jimen Bridge, Haidian District, Beijing**<br>**100088, China**<br>Facsimile No. **(86-10)62019451** | Authorized officer<br>**TANG,Shaohua**<br>Telephone No. **62086925** |

**INTERNATIONAL SEARCH REPORT**
**Information on patent family members**

International application No.
**PCT/CN2022/093013**

| Patent document cited in search report | | | Publication date (day/month/year) | Patent family member(s) | | | Publication date (day/month/year) |
|---|---|---|---|---|---|---|---|
| CN | 106467685 | A | 01 March 2017 | None | | | |
| CN | 107033650 | A | 11 August 2017 | None | | | |
| CN | 103443042 | A | 11 December 2013 | EP | 2691344 | A2 | 05 February 2014 |
| | | | | WO | 2012135294 | A2 | 04 October 2012 |
| | | | | JP | 2014511814 | A | 19 May 2014 |
| | | | | TW | 201245089 | A | 16 November 2012 |
| | | | | US | 2015208664 | A1 | 30 July 2015 |
| | | | | KR | 20140023328 | A | 26 February 2014 |
| | | | | US | 2014017462 | A1 | 16 January 2014 |
| CN | 110283529 | A | 27 September 2019 | None | | | |
| CN | 111185170 | A | 22 May 2020 | None | | | |
| CN | 110407482 | A | 05 November 2019 | None | | | |